# Insights from topo-bathymetric and oceanographic dataset for coastal flooding studies: The French Flooding Prevention Action Program of Saint-Malo

Léo Seyfried[1,3], Laurie Biscara[2], Héloïse Michaud[1], Fabien Leckler[2,4], Audrey Pasquet[1], Marc Pezerat[2], and Clément Gicquel[2]

[1]Shom, 42 Avenue Gaspard Coriolis, BP 45017 - 31032 Toulouse CEDEX 5, France
[2]Shom, 13 rue du Chatellier, 29200 Brest, France
[3]Exail robotics SAS, ZI Toulon EST, 262 Rue des Frères Lumière, 83130 La Garde
[4]France Energies Marines, 25 Avenue Alexis de Rochon, 29280 Plouzané, France

**Correspondence:** Héloïse Michaud : heloise.michaud@shom.fr

**Abstract.** The Action Program for Flood Prevention of Saint-Malo, France, requires the assessment of coastal flooding risks and the development of a local flooding warning system. The first prerequisite is a knowledge of the topography and bathymetry of the bay of Saint-Malo; the acquisition of new multibeam bathymetric data was performed in 2018 and 2019 to increase the resolution of the existing topo-bathymetric datasets and produce two high resolution (20 m and 5 m) topo-bathymetric digital terrain models. Second, the hydrodynamics associated with coastal flooding were investigated through a dense and extensive oceanographic field experiment conducted during winter 2018-2019, using a network of 22 moorings with 37 sensors: the network included 2 directional buoys, 2 pressure tide gauges, 18 wave pressure gauges, 4 single-point current meters, 7 current profilers and 4 acoustic wave-current profilers from mid-depth (25 m) up to the upper beach and the dike system. The oceanographic dataset thus provides an extended overview of hydrodynamics and wave processes in Saint-Malo bay, from the coast up to over-flooding and overtopping areas. It helps to identify the physical drivers of the coastal flooding, and provides a quantification of their respective contributions. In particular, the wave processes at the foot of the protection structures can be observed: in this macro-tidal environment, during high spring tides, short and infragravity waves propagate up to the protection structures, while the wave set-up remains negligible, and overtopping by sea packs can occur. The combination of high-resolution topo-bathymetric and oceanographic datasets allows the construction, calibration and validation of a wave and hydrodynamic coupled model that is used to investigate more deeply flooding processes, and might be integrated in a future local warning system by Saint-Malo intercommunality.

The topo-bathymetric and oceanographic datasets are available freely at doi : https://doi.org/10.17183/MNT_COTIER_GNB_PAPI_SM_20m_WGS84, https://doi.org/10.17183/MNT_COTIER_PORT_SM_PAPI_SM_5m_WGS84 and https://doi.org/10.17183/CAMPAGNE_OCEANO_STMALO (Shom, 2020a, b, 2021).

# 1 Introduction

## 1.1 Context

In the context of global warming, with a sea level rising and increased frequency of extreme events (Fox-Kemper et al., 2021), the growth of population and economic activity in areas at risk increases the vulnerability to coastal flooding (Crossland et al., 2005). Public policies need therefore to rely on scientific studies on coastal flooding risks in order to make the most relevant decisions on urban planning or safety.

In France, since the major coastal flooding event caused by the storm Xynthia (Bertin et al., 2012) in 2010, the government has strengthened policies to prevent the risk of coastal flooding. Shom (a public administrative institution supervised by the Ministry of the Armed Forces, www.shom.fr) develops, in collaboration with the French meteorological service Météo-France, the numerical forecasting systems that support the operational warning system for storm surges, in the scope of the HOMONIM project (Jourdan et al., 2020). At smaller scales, local territories develop initiatives that contribute to the national program 'Flooding Prevention Action Programs' (PAPI). These programs aim to promote a comprehensive and balanced approach to flood risk management tailored to specific territories and hazards within a coherent risk area. To increase scientific knowledge and public awareness of the coastal flooding hazard, Saint-Malo intercommunality urban area (SMA) has established a preliminary PAPI, in which the Shom participates, as a national partner in support of public policies for the sea and the coasts. The Shom's contribution is based on various actions including:

- the realization of in-situ oceanographic and bathymetric sea campaigns during the winter of 2018-2019 in order to produce up-to-date Topo-Bathymetric Digital Terrain Models (TBDTMs) as well as a characterization of physical properties of the coastal zone;

- the creation of a 42-year climatological hindcast to enable the definition of criteria for classifying high-risk storms and the calculation of joint return periods for static water-height and waves to characterize meteocean conditions favorable to coastal flooding and define warning thresholds;

- the generation of a very high-resolution coupled modeling system in Saint-Malo to model the storm surge and to consider in the medium term, an operational local flooding forecast system.

This document describes and analyzes the first action: to provide and interpret a new set of topo-bathymetric and hydrodynamic datasets. The data acquired are a prerequisite for the following 2 actions.

Getting access to detailed topo-bathymetric data is already a priority for communities anticipating impacts and preparing strategies in response to coastal risks. As elevation data are critical to depict regions prone to climate change impacts, this need will keep on increasing. Building high resolution and up-to-date TBDTMs, combining very dense and recent measurements from both ship-mounted multibeam echosounder and airborne LIDAR (Light Detection and Ranging), has become a prerequisite for modeling and forecasting of hydrodynamic processes at local scale (Eakins and Taylor, 2010). Shom developed multi-scales DTMs along the metropolitan and overseas French coasts based on user's requirements (Biscara et al., 2016)

and on previous works (e.g., Eakins and Taylor, 2010; Eakins et al., 2011; Eakins and Grothe, 2014). This nested products line was intended to be implemented in coastal flooding forecast systems in the scope of HOMONIM and TANDEM (Hébert et al., 2014; Maspataud et al., 2015) projects. However, their diffusion on Shom's data portal facilitated their use for many other marine environment issues such as ecology, erosion, geology purposes (e.g., Furgerot et al., 2019; Tawil et al., 2019; Famin et al., 2020; Tew-Kai et al., 2020).

Characterization of physical properties of the coastal zone is needed for coastal flooding hazard assessments, and is done by acquiring oceanographic observations of the water level variation (Melet et al., 2020). The water level variation is due to a complex combination of processes occurring in the open ocean (linked to the climate changes or the general ocean circulation) and in the coastal zone that will be discussed here. In the coastal zone, the processes influencing water level variations are mainly caused by tides, trapped waves, atmospheric pressure and wind effects, steric effects, wave setup, swash, infragravity waves, and, more locally, river runoffs, basin oscillations and meteotsunamis (Woodworth et al., 2019; Dodet et al., 2019). Thus, assessing the flooding risk at a local scale requires the monitoring of several meteocean variables (water levels, currents and sea states) and quantifying some processes (like storm surge, offshore wave, wave set-up, infragravity wave, swash). Such a monitoring requires the establishment of extensive oceanographic campaigns. Shom is the referent for water level observations along the French coast through the tide gauge network REFMAR, and conducts numerous oceanographic campaigns for coastal to littoral areas monitoring and model validation (Filipot et al., 2013; Dodet et al., 2018; Michaud et al., 2023), making use of its expertise and ressources.

In order to improve the knowledge of coastal flooding risks in Saint-Malo bay, an extensive bathymetric and oceanographic campaign was performed in winter 2018-2019. The topo-bathymetric and oceanographic datasets are detailed in parts 2 and 3, respectively. Part 4 outlines how these datasets will be valued for the studies of oceanographic processes and in particular in the identification of the key processes that can be responsible for coastal flooding, and their contribution to the development of the coupled surge/wave model, expected as part of the project. Part 5 provides the datasets availability. Finally, part 6 gives conclusions and limitations of these datasets.

## 1.2   Field site

Saint-Malo bay is located in the southern part of the Norman-Breton gulf (Figure 1.a). This bay is subject to a semidiurnal mega-tidal regime (maximum tidal range of about 13 m, Shom 2015 (among the largest in Europe)) and the estuarine conditions are modified by the Tidal power plant (Cochet and Lambert, 2017). Tidal currents are oriented E-SE during the flow and W-NW during the ebb, the velocities ranging from 1 m/s in the bay to 5 m/s in the estuarine part (Dagorne, 1966, 1968). In most situations, the waves come from W-NW to N-NW directions, with significant wave heights up to 6 m offshore during winter storms. Due to the presence of numerous obstacles (islets, shoals, groins), the waves propagation in the bay is complex. Moreover, geomorphology is marked by the presence of sand and rocky areas in the shallow bay, and a mixture of gravel and pebbles offshore (Bonnot-Courtois, 2002) making a non-homogeneous dissipation of waves by bottom friction over the bay.

The meteorological conditions are characterized by the passage of low pressure systems and cold fronts (Caspar et al., 2007). These weather conditions generate storm surges and are accompanied by significant swells. Combined with high spring tides,
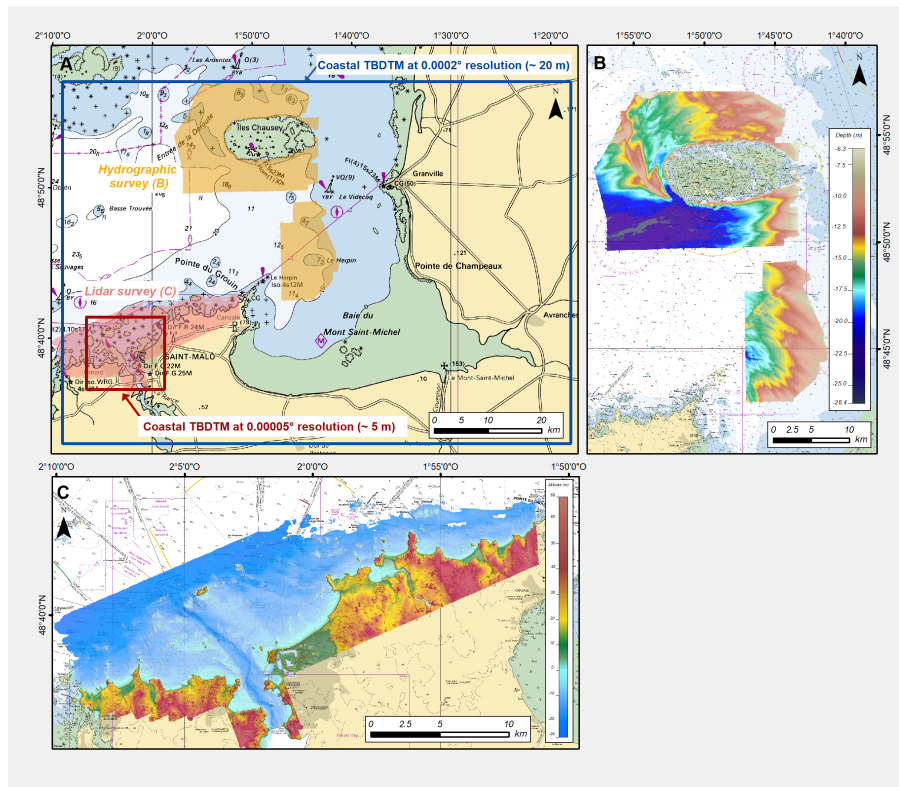
**Figure 1.** Nautical chart of Saint-Malo harbor and its surroundings (©Shom). (A) Locations of TBDTMs generated in the scope of Saint-Malo's PAPI project, (B) Bathymetric surveys carried out in the scope of PAPI Saint-Malo's project, (C) : Bathymetric coverage of Brittany v.20190831 Litto3D® maritime product of Saint-Malo harbor and its surroundings.

these events can lead to coastal flooding (Cariolet, 2011). Despite an existing dike system in front of Saint-Malo (Bonnot-Courtois, 2002), 8 storms events resulting in flooding or/and damage on the nearshore zone have been recorded in the literature between 1979 and 2019, and more than 40 have been identified since 1703 (DHI, 2016).

## 2   Topo-bathymetric dataset

90   The purpose of the following sections is to present the different data used for the generation of the TBDTMs (Figure 1.a), the most common problems experienced with combining data and the approach adopted by Shom for their resolution (Maspataud et al., 2015; Biscara et al., 2016).

**Table 1.** Survey start and end dates for the 3 bathymetric surveys.

| Bathymetric survey | Survey start date | Survey end date |
|---|---|---|
| La Pérouse (S201800400) | 30/01/2018 | 22/03/2018 |
| Laplace (S201805500) | 19/09/2018 | 12/10/2018 |
| Borda (S201901600) | 26/03/2019 | 24/04/2019 |

## 2.1 Data sources

### 2.1.1 Bathymetric Surveys

95  In the scope of the PAPI, the hydrographic vessels La Pérouse, Laplace and Borda were deployed between 2018 and 2019 in the Normand-Breton Gulf in order to update areas characterized precisely by a low resolution bathymetric coverage. The surveys covered approximately 230 km$^2$ in water depths ranging from -30 m to +6 m relative to the local chart datum (Figure 1.b). Table 1 details the schedule of the 3 bathymetric surveys carried out as part of the PAPI.

The hydrographic vessels are equipped with a Kongsberg-Maritime EM710 multibeam echo sounder associated with the SIS
100  acquisition system. Depending on the vessel, sound velocity profiles were measured using Sippican XBT probes or a Valeport SVP1000 Sound Velocity Profiler to correct bathymetric data for local variations in sound speed. Real time GPS positioning, roll, pitch and yaw information were collected with the Applanix POS MV inertial unit. Positioning data were post processed in POSPac software using global navigation satellite systems (GNSS) solutions. Horizontal positions were referenced to WGS84 or ITRF2014 geodetic systems at the time of the survey.

105  The bathymetric surveys were processed and qualified according to the IHO S-44 standard in effect at the time of the surveys were conducted (IHO, 2017a). Measured depths were corrected of various parameters (e.g. system calibration factors and sensor offsets, attitude corrections, sound velocity or tide values for the reduction of soundings). Subset editing was carried out by a qualified hydrographer (FIG/OHI/ICA cat. B, (IHO, 2017b)) using CARIS HIPS&SIPS 9.1 to remove systematic errors and outliers. Processed and cleaned data were subjected to final validation by a senior qualified hydrographer (FIG/OHI/ICA
110  cat. A,(IHO, 2018)). The Total Vertical Uncertainty (TVU, (IHO, 2017a)) of these surveys at the 95% confidence level is equal to 0.5 m. The Total Horizontal Uncertainty (THU, (IHO, 2017a)) at the 95% confidence level is between 0.55 m and 3.1 m. With a minimum overlap between adjacent lines of more than 50% of the half-swath, the 3 bathymetric surveys are compatible with orders 1a and 1b of the IHO S-44 standard.

### 2.1.2 Lidar data

115  LIDAR surveys exploited in this study were carried out within the framework of Litto3D® program. This national program is based on a partnership between Shom and the French National Geographic Institute (IGN) (Louvart and Grateau, 2005). It aims to provide very high resolution coastal altimetric models of metropolitan and overseas French coasts (Pastol, 2011). Litto3D® surveys are regularly implemented on Shom's data portal (data.shom.fr) under Open Licence. Coastal mapping of the

Normand-Breton Gulf was performed by Shom's Litto3D® team between 2016 and 2018, covering approximatively 700 km2
and reaching up to 18 m water depth (Figure 1.c). Topo-bathymetric data were acquired from a Cessna Grand Caravan 208B
type aircraft equipped with an airborne lidar topo-bathymetric HawkEye III double hatch (Leica Geosystems). The data were
acquired in relation to the ellipsoid and referenced horizontally with respect to the RGF93 in standard UTM 30N projection.
The trajectory of the aircraft was based on the GNSS system and processed by Inertial Explorer. The trajectory data were post-
processed using the stations of the RBF (Réseau de Base Français). The points were generated from the processed waveform
with Lidar Survey Studio (LSS) and the point cloud was processed using PFMABE version 6.4.0.43 tools. The validation of the
cleaned data was finally done by qualified hydrographers. Final point cloud data were finally reported to the IGN69 altimetry
reference frame and to the Lambert 93 projection by the Circe Batch (V4-3, Using RAF09 model) conversion tool.

### 2.1.3   Shom's bathymetric database

Complementary bathymetric data used to generate the TBDTMs were extracted from the Shom's bathymetric database (BDBS).
52 bathymetric surveys (490 millions of soundings) conducted between 1829 and 2019 with different sounding methods (lead-
lines, single beam and multibeam echosounders) were available on the area of interest. Each survey extracted from the BDBS
is associated with metadata, including the acquisition and processing methods, the IHO order survey and the quality of the
data. Spatial coverage of each survey is represented as a vector polygon layer (called hereafter bounding polygon) that may
adjoin, overlap or supersede older bathymetric surveys.

### 2.1.4   Other data

In addition to these bathymetric data, a bathymetric survey of the inner harbor delivered by the harbor authority of Saint-Malo
was used in the present study. The bathymetric survey was carried out in June 2016 by the GEOXYZ society with a multibeam
echosounder. Soundings were vertically referenced to the chart datum of Saint-Malo. This bathymetric source was evaluated
prior to integration to other datasets.

The RGE ALTI® V2.0, produced by IGN, was exclusively used for the terrestrial domain. The data are available on the
IGN's data portal (https://geoservices.ign.fr) in the RGF93 geodetic system, Lambert 93 projection. Vertical datum of the data
corresponds to the NGF-IGN69 legal system (IGN, 2018). The RGE ALTI® v2.0 products used in the TBDTMs cover the
departments of Côtes d'Armor, Ille et Vilaine and Manche at a resolution of 5 m. Data was clipped with a buffer extending to
3 km inland. Water-surface values were also eliminated using the raster layer of sources provided with the DTMs.

### 2.2   Production process

### 2.2.1   Convert data to a common horizontal and vertical datum

The key requirement for creating a seamless merged product is the homogeneity of the input datasets in terms of horizontal
and vertical datum (Gesch and Wilson, 2001). The vertical transformation to the ellipsoid was performed with Circe 5.1 France
(IGN) and Bathyelli V2.0 (Shom) for topographic and bathymetric data, respectively.

### 2.2.2 Data compilation

Selecting the most reliable source from multi-temporal and multi-sensor data is a fundamental challenge addressed in numerous works (Macnab and Jakobsson, 2000; Wong et al., 2007; Maspataud et al., 2015). This is particularly true for hydrographic offices, such as the Shom, which have a considerable legacy of data. Bathymetric data has been collected using several sounding methods with specific characteristics of accuracy and precision.

Due to the scarcity and the difficulty of collecting bathymetric data, TBDTMs are produced from a process of data compilation. This process, also known as "deconfliction", aims to ensure that the most relevant sources are selected to create the best possible representation. Until now, this tedious process was carried out manually in accordance with the S-44 standard and survey specifications (Maspataud et al., 2015; IHO, 2017a). To make it more efficient, Shom initiated in 2019 the Téthys project (Figure 2). This in-house project aimed at constituting Shom's bathymetric layer surface for which source data have been selected in order to generate the most accurate and up-to-date surface, satisfying the criteria related to the safety of navigation (Le Deunf et al., 2023). Overlap conflicts between surveys are resolved by a set of decision rules exploiting metadata (e.g. date, density, uncertainty and IHO order) which define if a survey supersede or complete older ones (Figure 2.b). In case of a survey with a "supersede" status, the deconfliction process is executed by clipping the bounding polygon of the reference survey to all other older overlapping surveys. No clipping is done for surveys with a "complete" status (Figure 2.b). The resulting layer will be regularly updated on the basis of newly integrated surveys (Figure 2.c).

The generation of TBDTMs in the Normand-Breton gulf benefited from the reliability of all metadata and bounding polygons in the area of interest, which constitute the preliminary step prior to the construction of the Téthys. The deconfliction process was executed on all datasets used for the generation of the TBDTMs using routines based on modules (selection, filtering, masking, merging) available with GMT 5.1.1. (Wessel et al., 2013). The result of the deconfliction process corresponds to the most reliable soundings that can be used as input into the surface modeling.

### 2.2.3 Interpolation

Because multiple sources of data contribute to the construction of the DTM, some datasets have data point spacing larger than the required cell size. Splines functions are generally used for their efficiency when data densities vary. They produce a representative smooth and continuous surface. There may be more appropriate for large interpolation distances, which is frequently required for bathymetric data (Amante (2012) and references therein). Based on these observations, Shom used the SAGA (System for Automated Geoscientific Analyses; Conrad et al. (2015)) software packages for the generation of the TBDTMs. Multilevel B-splines interpolation tool was used to perform surface modelling of the compiled data.

### 2.2.4 Altimetric conversion grids

Following NOAA's previous works (Eakins and Taylor, 2010; Eakins et al., 2011), different datum altimetric grids were developed by Shom to convert the TBDTMs from the ellipsoid to other tidal datums (Lowest Astronomical Tide and Mean Sea Level). The creation of vertical reference surfaces at sea, linked to the ellipsoid, was initiated for metropolitan France with the
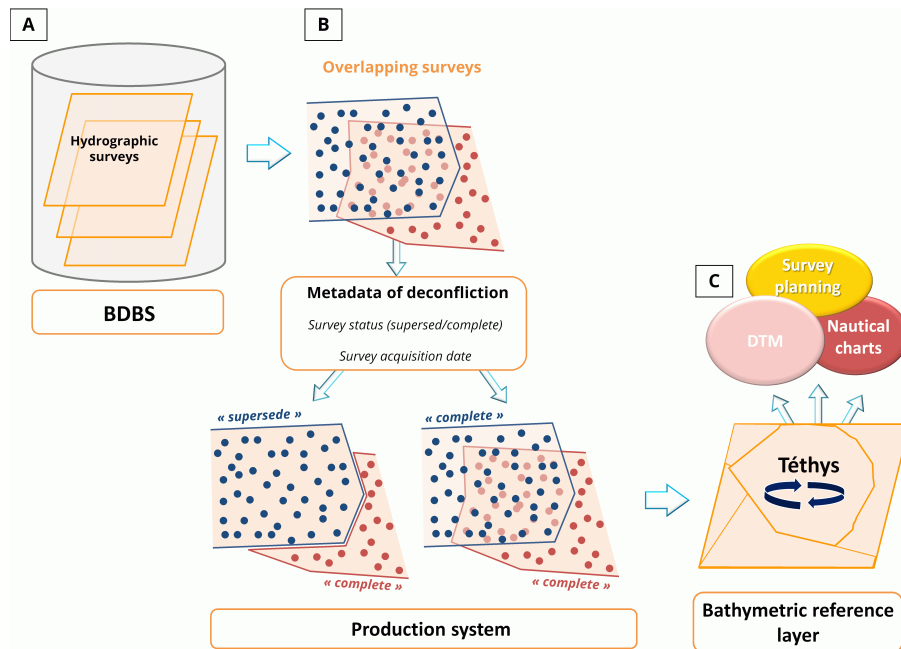
**Figure 2.** Workflow of Shom's bathymetric reference layer (« Téthys »). (A) Shom's bathymetric knowledge is composed of numerous overlapping surveys that are compiled in the BDBS. (B) In the case of overlapping surveys, a conflict resolution is applied based on the metadata of deconfliction. For bathymetric surveys which supersede older ones, the bounding polygon is used to clip the data. For bathymetric surveys which complete older ones, no action is performed. (C) Deconflicted data are compiled in one bathymetric reference layer for different applications. The reference layer will be updated each time a new survey is integrated in the BDBS.

"BATHYELLI" project (Pineau-Guillou and Dorst, 2013). The surface realizations used to convert TBDTMs correspond to the propagation of a vertical sea reference to all points in a tidal zone, using a tidal model and a concordance equation.

### 2.2.5 Evaluation

185 The various checks carried out on the Téthys layer (reliability of attributes and bounding polygons, spatial coherence...) provide a robust data compilation from which the bathymetric surface is modeled. The DTM is equally evaluated with qualitative and visual inspection (slope, cross-section and 3D views) and through additional layers (density, sources diagram). If possible, a cross-validation of the DTM with datasets that have not been incorporated into the generated product due to diffusion constraints is made. Despite the processing efforts and the deconfliction process, erroneous representation of the sea-floor may
190 remain. Preliminary versions of the TBDTMs highlighted two different types of artifacts:

- the overlapping of some bathymetric surveys with a "complete" status, leading to a noisy representation of the seafloor. In this case, the surface will not be suitable for modeling purposes despite the consistency of the surveys with each other in respect to the S-44 standard. Therefore, the survey with the strongest TVU is clipped to generate a coherent surface.
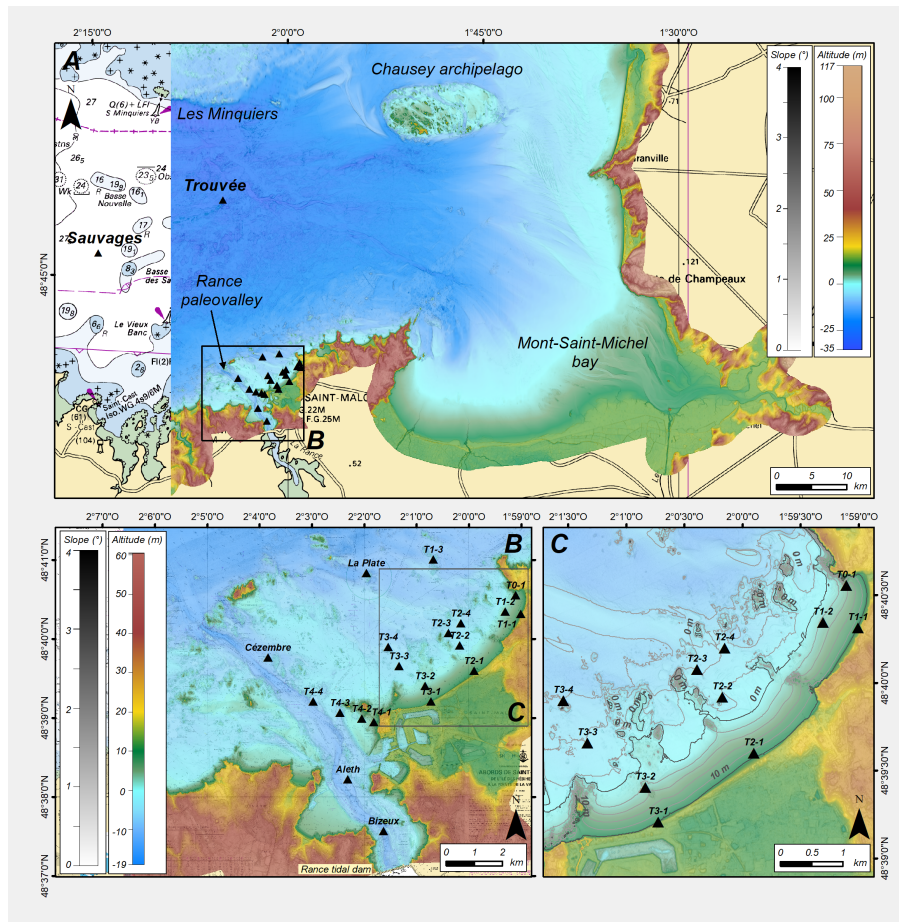
**Figure 3.** Nautical charts of Saint-Malo bay and its surroundings (©Shom). (A) coastal TBDTM covering a part of the Normand-Breton gulf at a resolution of 0.0002° (~20 m and moorings positions); (B) coastal TBDTM of the harbor of Saint-Malo and its surroundings at a resolution of 0.00005° (~5 m) moorings positions. (C) Zoom on the sensors transects.

    – an erroneous representation of depth can occur when three-dimensional data are far away, especially in unsurveyed
195       marine areas (Eakins and Grothe, 2014; Danielson et al., 2016). In this configuration, the optimal fit of the B-spline
       multilevel model is not sufficiently constrained, the least-squares minimization is ill-posed and the resulting model can
       generate unwanted oscillations. Locally, these artifacts are minimized by increasing tension factor to smooth the surface.

As long as anomalies are detected, their cause must be determined and data reprocessed prior to a new interpolation. These different steps must be repeated iteratively until a satisfactory result is reached (Eakins and Taylor, 2010).

## 2.3 Morphological description

Although the creation of TBDTMs is only a prerequisite for the flood forecasting model, it also enables us to describe the main morphological characteristics of the area under study. For the Saint-Malo harbor and surrounding area, the TBDTM covers an area of 85 km$^2$ (Figure 3.b). At its center lies the mouth of the Rance, reaching a depth of around 10 m, 3 km downstream of the tidal power plant. The estuary extends further north, near Cézembre Island, through an incision in the coastal shelf along which the depth reaches 15 m. At the east of the estuary, there is an important accumulating bedform, the bench of Pourceaux, made of coarse sands (Bonnot-Courtois, 2002). The rest of the foreshore is characterized by smaller marine sedimentary deposits and submerged rocky structures, which provide partial protection from the prevailing north-westerly swells. In fact, it is considered as an abrasion platform that evolves under very high hydrodynamic conditions and consequently has a poorly developed sedimentary prism (Daire et al., 2014). Apart from harbor infrastructures, the intertidal zone is characterised by sandy beaches in between rocky outcrops. The beaches are relatively small, with the largest, the Sillon beach, that stretches along 3 km across a former marsh, on which a large part of Saint-Malo is located. The beach is topped by a protective structure, the Paramé dyke. Built in the 19th century initially to protect industries and then the burgeoning seaside resort located in low-lying areas from erosion and flooding, the dike has suffered extensive storm damage over the years, and has been repaired and remodeled many times over. On the TBDTM, the height of the dyke varies now between 14.3 m and 15.8 m above chart datum. However, in spite of the attempts to manage the coastal landscapes and the position of the coastline with dykes and embankments over the years, the shoreline has changed and will still evolve, due to expected climatic and meteorological changes. Thus, acquiring these new topobathymetric data within the framework of the PAPI provides a snapshot of the coastline at a given moment. Sediment balances can be conducted by comparing them to older measurements, enabling the assessment of vulnerability to marine risks in this climatic context. Furthermore, through modeling and hydrodynamic data acquisition, a more accurate evaluation of flooding risks will be obtained, leading to more effective planning of coastal protection measures.

## 3 Oceanographic dataset

The oceanographic dataset includes water levels, currents and sea states observations from extensive in situ measurements conducted by the Shom during winter 2018-2019, using different types of sensors. In the following the field campaign and the data processing are described.

### 3.1 Oceanographic Surveys

From October 2018 to April 2019, an extensive oceanographic campaign was conducted in Saint-Malo bay. The campaign includes 22 moorings, each mooring containing one or two sensors, for a total of 37 sensors :

- Two directional waveriders (Datawell, DWR-MkIII, hereafter referred to as Datawell)

- Two tide pressure gauges (Seabird Electronics, SBE26+, hereafter referred to as SBE)

230      – Four acoustic wave and current profilers (Nortek, AWAC 600 kHz, hereafter referred to as AWAC)

     – Four single-point current meters (Nortek, Aquadopp single-point current meter, hereafter referred to as Aquadopp)

     – Seven current profilers (Nortek, Aquadopp profiler 1 MHz, hereafter referred to as AquaPro)

     – Eighteen wave pressure gauges (Ocean Sensor System Inc., ten OSSI-010-003C and eight OSSI-010-022, hereafter referred to as OSSI and OSSI-NEW, respectively)

235      The moorings were located so as to accurately describe hydrodynamic conditions from offshore to the coastline (Figure 1). The Datawell were deployed offshore at 25 m-depth (Sauvages and Trouvée, Figure 1.a), providing information on the offshore wave fields. Other moorings were essentially deployed along four cross-shore transects (T1, T2, T3 and T4, figure 1.b). Around the transects T1, T2 and T3, the beach profile is characterized by a gentle foreshore slope (2 %, Figure 1.c), increasing slightly (3 %) on the eastern part of the Minihic beach (T0 sensor). Transect T4 is located in the vicinity of the Grand Bé islet and is
240 characterized by high slope variations due to the presence of the Rance estuary (Figure 1.b). Two moorings, with OSSI and AquaPro, were deployed in the Rance estuary (Bizeux and Aleth Figure 1.b). Table 2 summarizes the location of each mooring and sensor. For consistency with TBDTMs, the vertical datum used is the Lowest Astronomical Tide (LAT).

**Table 2.** Moorings and sensors location.

| Moorings | Sensors | Latitude (WGS84) | Longitude (WGS84) | Sensors depth (LAT) | Altitude (from seabed) |
|---|---|---|---|---|---|
| T0-1 | OSSI | 48.675893° | -1.985119° | -4.60 m | 0.19 m |
| T1-1 | OSSI | 48.671880° | -1.983443 | -10.58 m | 0.15 m |
| T1-2 | OSSI | 48.672397° | -1.988447° | -3.98 m | 0.35 m |
|  | AquaDopp |  |  | -4.34 m | 0.71 m |
| T1-3 | OSSI | 48.683417° | -2.011383° | 6,00 m | 0.32 m |
|  | AWAC |  |  | 5.70 m | 0.62 m |
| T2-1 | OSSI | 48.659966° | -1.998369° | -9.17 m | 0.11 m |
| T2-2 | OSSI | 4.665283° | -2.002883° | 1.88 m | 0.35 m |
|  | AquaDopp |  |  | 1.52 m | 0.71 m |
| T2-3 | OSSI | 48.667900° | -2.006517° | 4.09 m | 0.35 m |
|  | AquaPro |  |  | 3.73 m | 0.71 m |
| T2-4 | OSSI | 48.669933° | -2.002533° | 4.72 m | 0.35 m |
|  | AquaPro |  |  | 4.36 m | 0.71 m |
| T3-1 | OSSI | 48.653437° | -2.012057° | -11.36 m | - |
| T3-2 | OSSI | 48.656722° | -2.013924° | -3.67 m | 0.35 m |
|  | AquaDopp |  |  | -4.03 m | 0.71 m |
| T3-3 | OSSI | 48.660933° | -2.022233° | 4.16 m | 0.35 m |
|  | AquaPro |  |  | 3.80 m | 0.71 m |
| T3-4 | OSSI | 48.664967° | -2.025683° | 4.96 m | 0.35 m |
|  | AquaPro |  |  | 4.60 m | 0.71 m |
| T4-1 | OSSI | 48.649110° | -2.030283° | -5.93 m | 0.20 m |
| T4-2 | OSSI | 48.649900° | -2.034132° | -4.60 m | 0.35 m |
|  | AquaDopp |  |  | -4.96 m | 0.71 m |
| T4-3 | OSSI | 48.651117° | -2.041050° | 5.26 m | 0.35 m |
|  | AquaPro |  |  | 4.90 m | 0.71 m |
| T4-4 | OSSI | 48.653483° | -2.049600° | 5.77 m | 0.35 m |
|  | AWAC |  |  | 5.50 m | 0.62 m |
| Aleth | OSSI | 48.637033° | -2.038617° | 4.46 m | 0.35 m |
|  | AquaPro |  |  | 4.10 m | 0.71 m |
| Bizeux | OSSI | 48.626167° | -2.027150° | 9.36 m | 0.35 m |
|  | AquaPro |  |  | 9.00 m | 0.71 m |
| Cezembre | SBE | 48.662700° | -2.063933° | 6.00 m | - |
|  | AWAC |  |  | 5.90 m | 0.62 m |
| La Plate | SBE | 48.680533° | -2.032583° | 5.17 m | - |
|  | AWAC |  |  | 6.20 m | 0.62 m |
| Trouvée | DATAWELL | 48.813183° | -2.083483° | 25 m | - |
| Sauvages | DATAWELL | 48.768550° | -2.242817° | 25 m | - |

Sensors deployed during the campaign have been programmed to accurately record the oceanographic data, taking into account battery and data storage limitations. Sensors settings in terms of measurement data, sampling rate, average interval and measurement interval are summarized for each sensor in Table 3.

**Table 3.** Sensor acquisition protocol.

| Moorings | Sensors | Datas | Sampling rate | Average interval | Measurement interval | Remarks |
|---|---|---|---|---|---|---|
| T0-1 | OSSI | Bottom Pressure | 10 Hz | Continuous | Continuous | - |
| T1-1 | OSSI | Bottom Pressure | 10 Hz | Continuous | Continuous | - |
| T1-2 | OSSI | Bottom Pressure | 10 Hz | Continuous | Continuous | - |
| | AquaDopp | Current | - | 120 s | 600 s | - |
| | | Bottom Pressure | | | | |
| T1-3 | OSSI | Bottom Pressure | 10 Hz | Continuous | Continuous | - |
| | | Current | - | 120 s | 600 s | |
| | AWAC | AST | 2 Hz | 1024 s | 7200 s | - |
| | | Bottom Pressure | 2 Hz | 1024 s | 7200 s | |
| T2-1 | OSSI | Bottom Pressure | 8 Hz | Continuous | Continuous | Battery Problem |
| T2-2 | OSSI | Bottom Pressure | 8 Hz | Continuous | Continuous | Battery Problem |
| | AquaDopp | Current | - | 120 s | 600 s | - |
| | | Bottom Pressure | | | | |
| T2-3 | OSSI | Bottom Pressure | 8 Hz | 1800 s | 3600 s | Battery Problem |
| | AquaPro | Current | - | 120 s | 1200 s | - |
| | | Bottom Pressure | | | | |
| T2-4 | OSSI | Bottom Pressure | 8 Hz | 1800 s | 3600 s | Battery Problem |
| | AquaPro | Current | - | 120 s | 1200 s | - |
| | | Bottom Pressure | | | | |
| T3-1 | OSSI | Bottom Pressure | 8 Hz | Continuous | Continuous | Battery Problem Siltation |
| T3-2 | OSSI | Bottom Pressure | 8 Hz | Continuous | Continuous | Battery Problem |
| | AquaDopp | Current | - | 120 s | 600 s | - |
| | | Bottom Pressure | | | | |
| T3-3 | OSSI | Bottom Pressure | 8 Hz | 1800 s | 3600 s | Battery Problem |
| | AquaPro | Current | - | 120 s | 1200 s | - |
| | | Bottom Pressure | | | | |
| T3-4 | OSSI | Bottom Pressure | 8 Hz | 1800 s | 3600 s | Battery Problem |
| | AquaPro | Bottom Pressure | - | 120 s | 1200 s | - |
| T4-1 | OSSI | Bottom Pressure | 10 Hz | Continuous | Continuous | - |
| T4-2 | OSSI | Bottom Pressure | 10 Hz | Continuous | Continuous | - |
| | AquaDopp | Current | | 120 s | 600 s | - |
| | | Bottom Pressure | | | | |
| T4-3 | OSSI | Bottom Pressure | 10 Hz | 1800 s | 3600 s | Mooring Lost |
| | AquaPro | Current | | 120 s | 1200 s | |
| | | Bottom Pressure | | | | |
| T4-4 | OSSI | Bottom Pressure | 10 Hz | 1800 s | 3600 s | - |
| | | Current | - | 120 s | 600 s | |
| | AWAC | AST | 2 Hz | 1024 s | 7200 s | - |
| | | Bottom Pressure | 2 Hz | 1024 s | 7200 s | |
| Aleth | OSSI | Bottom Pressure | 10 Hz | 1800 s | 3600 s | - |
| | AquaPro | Current | - | 120 s | 1200 s | - |
| | | Bottom Pressure | | | | |
| Bizeux | OSSI | Bottom Pressure | 10 Hz | 1800 s | 3600 s | - |
| | AquaPro | Current | - | 120 s | 1200 s | - |
| | | Bottom Pressure | | | | |
| Cézembre | SBE | Bottom Pressure | 4 Hz | 120 s | 1200 s | - |
| | | Current | - | 120 s | 600 s | |
| | AWAC | AST | 1 Hz | 1024 s | 3600 s | - |
| | | Bottom Pressure | 1 Hz | 1024 s | 3600 s | |
| La Plate | SBE | Bottom Pressure | 4 Hz | 120 s | 1200 s | - |
| | | Current | - | 120 s | 600 s | |
| | AWAC | AST | 2 Hz | 1024 s | 7200 s | Sensor disconnected |
| | | Bottom Pressure | 2 Hz | 1024 s | 7200 s | |
| Trouvée | DATAWELL | Displacement | 1.28 Hz | Continuous | Continuous | - |
| Sauvages | DATAWELL | Displacement | 1.28 Hz | Continuous | Continuous | - |

### 3.1.1 Sensor acquisition

Figure 4 presents a summary report of sensor acquisition. All moorings, except buoys, started on november, the 12th 2018. The last acquisitions were March 30 and April 20 for foreshore or offshore moorings, respectively. The acquisitions of Datawell buoys began on November 15, 2018, for Trouvée mooring and on December 2, 2018, for the Sauvages mooring, until April 29, 250   2019, for both buoys. Figure 4 shows interruptions in data acquisition for OSSI-NEW in transects T2 and T3. These interruptions were caused by less efficient batteries than anticipated on the OSSI-NEW's (as mentioned in table 3). For moorings on the foreshore, a brief interruption in the data acquisition appeared from January 22 and January 24. This interruption was planned for a battery change. The "La Plate" AWAC sensor did not acquire any data during the campaign (the sensor power cable was disconnected). The mooring T4-3 with all the sensors remains unfortunately unrecovered, problably due to a malicious act. 255   Despite these incidents, the density and complementarity of the instruments used during the campaign give an homogeneous description of the hydrodynamics in Saint-Malo bay. The data collection covers a winter period of more than 4 months.
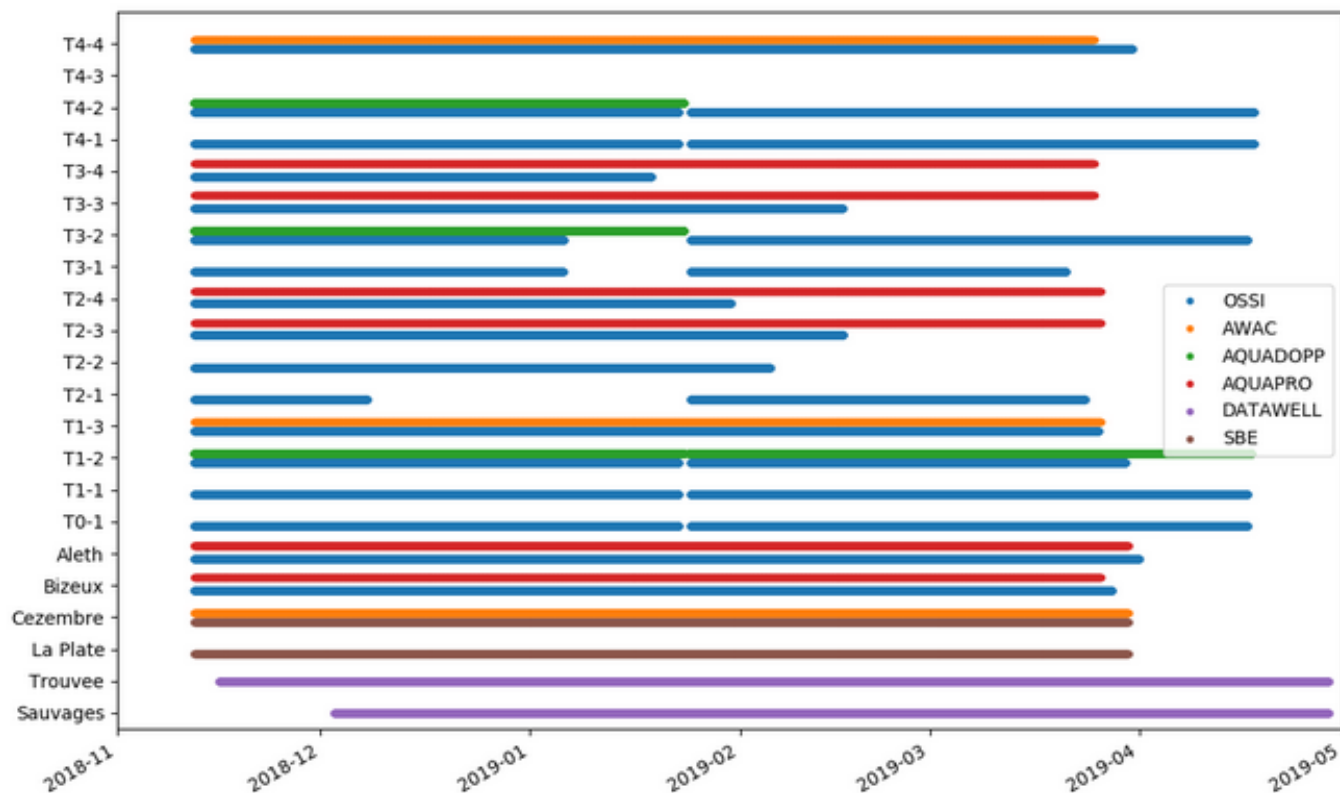
**Figure 4.** Moorings acquisition report.

### 3.2 Data processing

The workflow for generating the oceanographic dataset consists of three steps:

- Pre-process binary data using the manufacturers' software.

260     – Process the data using the Python toolbox SCOT developed for this study.

- Write data, metadata to netcdf format.

### 3.2.1 Water levels

The water levels are mainly monitored by pressure sensors including tide pressure gauge (SBE) and wave pressure gauge (OSSI) using different sampling frequencies and acquisition plans (Table 3). Current meters (Aquadopp, Aquapro or Awac)

265   are also equipped with pressure sensors.

The tide pressure gauges also record the 2 min-averaged bottom pressure every 20 minutes. The raw data was converted in water level $h$ assuming hydrostatic equilibrium (Eq. 1):

$$h = \frac{P_m - P_{atm}}{\rho g} + \delta_m \tag{1}$$

270   with $P_m$, the bottom pressure measurement in Pa, $P_{atm}$, the atmospheric pressure extracted from ERA5 atmospheric reanalysis in Pa, $\rho = 1026\,\mathrm{kg}/m^3$, the averaged water density measured in Saint-Malo bay, $\delta_m$ the sensor's distance from bed in m and $g = 9.81$ m/$s^2$ the gravitational acceleration. Note that the data from ERA5 reanalysis were preferred to measurements at Dinard airport meteorological station due to acquisition problems.

275   The wave pressure gauges and current meter with pressure sensors record bottom pressure at higher frequency (see Table 3). In case of continuous measurements, the data recorded in ascii format were aggregated in consecutive bursts of prescribed length (20 min here). The raw pressure data of each sensor is calibrated using the pressure slope and offset of the sensor. For foreshore sensors, the calibration is performed by comparing the burst-averaged pressure measured whenever the sensor is out of water to the atmospheric pressure (e.g. see Appendix C). For offshore sensors, the pressure sensor was calibrated before

280   or at the end of the recording when the instrument was taken out of the water. Then, the corrected pressure was converted into water level assuming hydrostatic equilibrium (Eq. 1). Finally, to reconstruct water level for the long waves such as tide, the water level was smoothed, with moving average of 10 min, to filter out deformations of water surface related to short waves.

In order to compare water levels recorded from different instruments, the measurements were relocated in height with respect

285   to the tide gauge of Saint-Malo harbour (e.g. see Appendix C). The correction factors (slope and offset) from Saint-Malo tide gauge is provided in the dataset for each sensor. The accuracy of water levels is in the order of $\pm 5$ cm. For consistency with TBDTMs, the vertical datum used is the Lowest Astronomical Tide (LAT).

Finally, acoustic surface tracking (AST) with vertical beam performed by AWAC current meters allow the sampling of the surface elevation.

### 3.2.2 Currents

The currents are monitored by acoustic Doppler current using single-point current meters (Aquadopp) and current profilers (AquaPro and AWAC). These sensors record the speeds in the axis of their three beams. The raw binary data file was directly processed by the Python toolbox SCOT developed for this study. First, the velocity data are reprojected in a terrestrial landmark, on the north-east-vertical axes. Prior to their deployment, the magnetic compasses of these current meters were previously calibrated on a dedicated Shom platform. The calibration procedure and the uncertainty of current data are described in Le Menn and Morvan (2020). Finally the current data and metadata of each sensor are written in netcdf format.

### 3.2.3 Sea States

The sea states are monitored by three different types of sensor: directional wave buoy, wave pressure gauge, and acoustic wave and current profiler.

The directional wave buoys recorded wave displacements in the three directions of the ENU frame using measurements from accelerometers, inclinometers and compass. First, a quality control is performed on each 30 min bursts, such that a burst is discarded if at least one of the three displacements is outside the range $\pm 4\sigma$ where $\sigma$ is the standard deviation of the timeseries. Then, the cross-spectra of the displacements were computed by means of a Fast Fourier Transform (FFT) on 10 hanning-windowed segments with a 50% overlap, which allows a good compromise between statistical stability (20 degrees of freedom) and frequency resolution (5.5 mHz). The power spectral density of vertical displacements are used for estimating the main bulk parameters (see Appendix B), while the five other independent co- and quad-spectra are used to compute the main directional parameters and estimate the directional distribution using the Iterative Maximum Likelihood Method with an angular resolution of $5°$ (e.g., see Oltman-Shay and Guza, 1984) so as to compute an estimate of the directional spectra.

For the wave pressure gauges, the free surface elevation signal associated with waves was first reconstructed from bottom pressure measurements so as to account for the non-hydrostatic effects. A recent review of Mouragues et al. (2019) provides different methods depending on the assumptions made on the wave field's dispersive properties. In addition to the hydrostatic reconstruction, the linear method and non-linear weakly dispersive method (see Appendix A) were thus applied on each burst after detrending so as to suppress tidal motion. The wave spectra were computed as described above (resulting in 20 degrees of freedom and a frequency resolution of 5.5 mHz) to finally compute spectral estimates of the bulk parameters in addition to the wave-by-wave analysis (see Appendix B).

The AWAC records surface elevation from Acoustic Surface Tracking (AST) and the two components of the horizontal current in the ENU frame within a sub-surface wave cell at high frequency. First, a quality control is performed on each burst

based on the QC-flag associated with AST measurements, such that a burst is discarded when the first quartile of the QC-flag distribution is below 100, which corresponds to the ceil below which the measurement is considered dubious (Nortek support team personal communication). Then, the cross-spectra of the measurements triplet were computed as described above (resulting in 20 degrees of freedom and a frequency resolution of 7.8 mHz) and the same processing as for the directional wave buoy measurements is performed (e.g. see Krogstad et al., 1988, for the estimate of the directional distribution from ADCP measurements using the IMLM method).

## 4 Applications of these dataset

Section 4 aims at bringing some insights on the benefits of such datasets. The first one is to understand, identify and quantify key processes of coastal flooding. A second benefit is that they are crucial to the development as well as the calibration/validation of a high-resolution coupled surge/wave model, which is expected as part of the preliminary PAPI study.

## 4.1 Overview of oceanographic processes
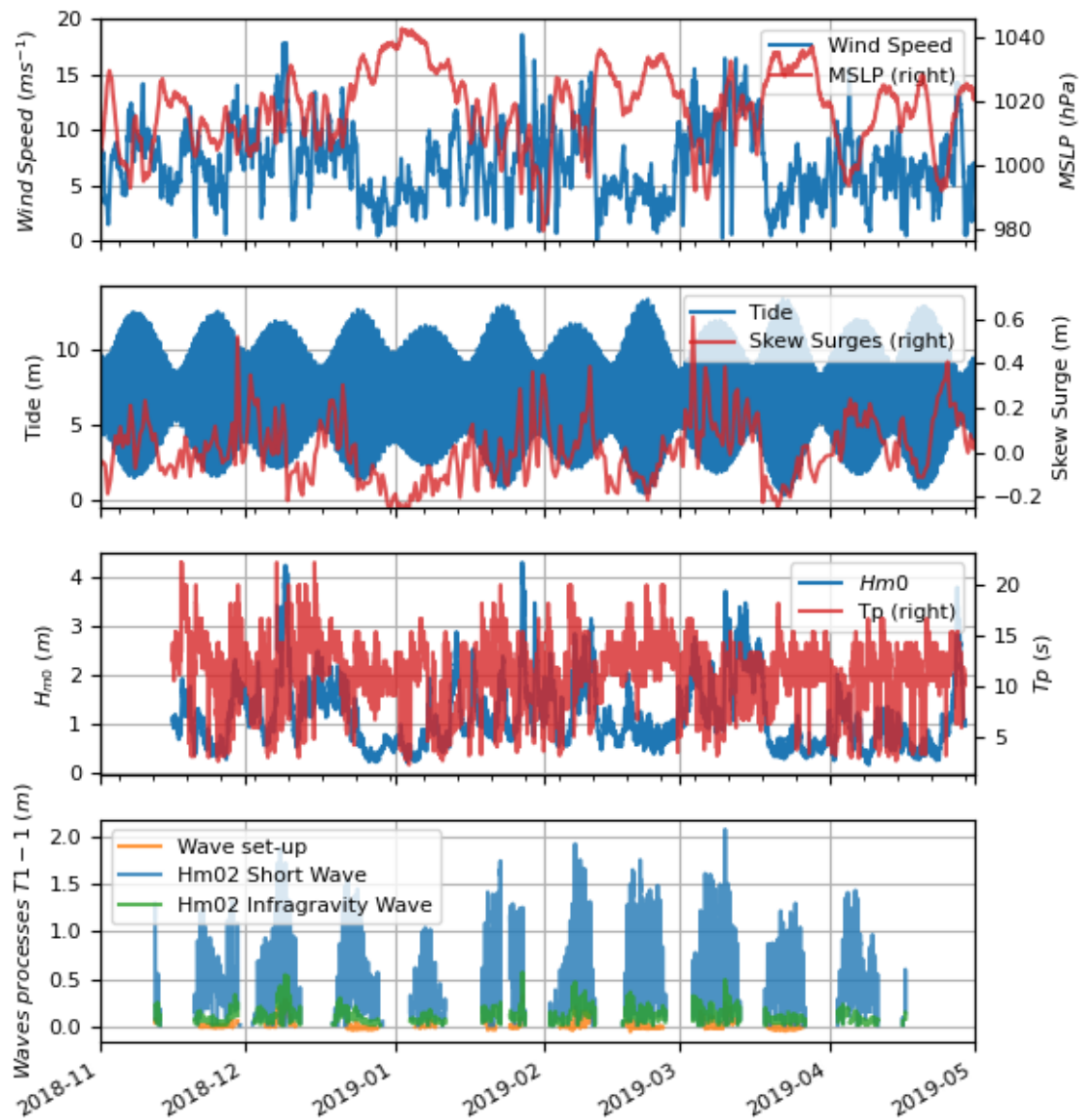
**Figure 5.** (A) wind speed and Mean Sea Level Pressure (MSLP) from ERA5 reanalysis in Saint-Malo. (B) Tide prediction and skew surge at Saint-Malo harbour tide gauge. (C) Significant wave height $H_{m0}$ and peak period at Trouvée buoy. (D) Short and infragravity significant waves height, and wave set-up at T1-1 .
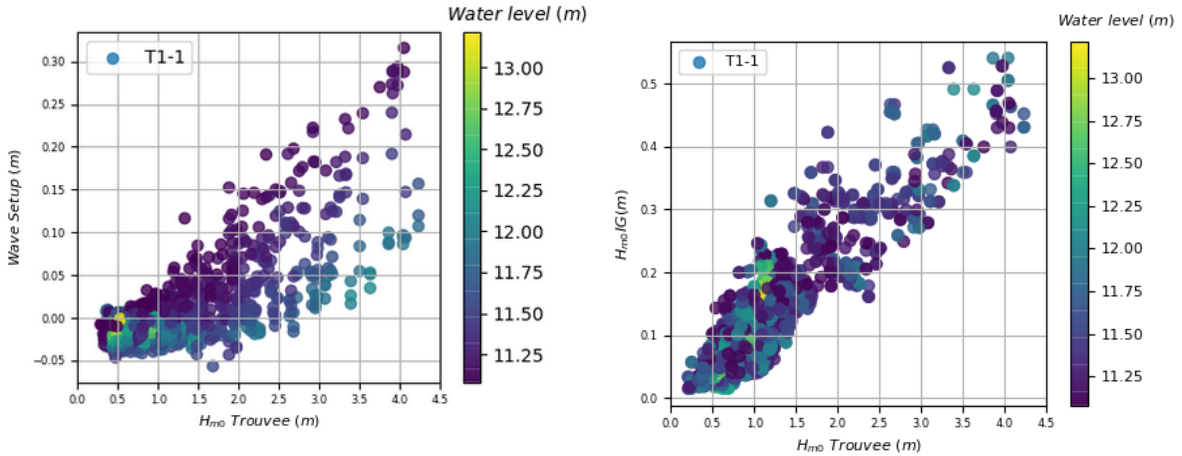
**Figure 6.** Wave set-up (left) and infragravity significant wave height (right) at T1-1 mooring according to offshore significant wave height and water level (color).

**Table 4.** Inventory of metocean conditions (Wave conditions at Trouvée) and waves processes at T1-1 during storm events and major spring tide events of field experiment.

|          | MSLP (hPa) | Wind speed (m/s) | Hm0 offshore (m) | Tp offshore (s) | Height Tide (m) | Skew Surge (cm) | Set-up (cm) | Short Waves (cm) | Infragravity Waves(cm) |
|----------|------|------|------|----|-------|-----|----|-----|-----|
| 29/11/18 | 1003 | 14   | 2.29 | 18 | 10.59 | 53  | 4  | 110 | 25  |
| 09/12/18 | 1011 | 18   | 4.24 | 11 | 11.80 | 22  | 27 | 173 | 54  |
| 27/01/19 | 991  | 18   | 4.28 | 11 | 10.91 | 29  | 32 | 128 | 52  |
| 10/02/19 | 996  | 15   | 3.08 | 8  | 10.98 | 39  | 15 | 130 | 24  |
| 21/02/19 | 1032 | 3    | 1.0  | 10 | 13.17 | -10 | 0  | 136 | 12  |
| 03/03/19 | 994  | 15   | 2.75 | 14 | 10.01 | 61  | -  | -   | -   |
| 10/03/19 | 1011 | 16   | 3.73 | 11 | 11.70 | 33  | 24 | 207 | 50  |
| 22/03/19 | 1030 | 4    | 0.7  | 14 | 13.33 | -15 | 0  | 82  | 6   |

The figure 5A-C shows an overview of the temporal evolution of the metocean conditions during the studied period. First, several low-pressure systems affected Saint-Malo. These storm events produced skew surges (that is the difference between the maximum observed sea level and the maximum predicted tide regardless of their timing during the tidal cycle) from 22 cm 335 to 61 cm and offshore significant wave heights from 2.29 m to 4.28 m. These storms occur principally during neap tides. No coastal flooding was observed during this experiment. The storm events associated with two major spring tides are reported in Table 4 with the corresponding metocean conditions.

The wave transformation induces further processes affecting water level elevation such as wave set-up and infragravity waves (e.g. see Dodet et al., 2018). The figure 5D shows the wave set-up estimated from the difference of water level between sensor T1-1 and T1-2 and infragravity significant wave height (between 0.004 and 0.04 Hz) at T1-1. The maximum wave set-up was measured during the 09/12/18, 27/01/2019 and 10/06/19 storms with wave set-up measurement of around 27 cm, 32 cm and 24 cm, respectively. The maximum infragravity significant wave heights also occur during these storms with heights greater than 50 cm. Table 4 indicates the wave set-up, short and infragravity significant wave heights at T1-1 for each storm concomitant with spring tide event. The figure 6 shows the wave set-up estimates and the infragravity significant wave height versus the offshore significant wave height associated with the corresponding water levels. The wave set-up and the infragravity significant wave height increase with the offshore significant wave height as expected. The wave setup appears closely related to the water level, with higher wave setup at rising and falling tide whereas at high tide (sea levels > 12 m), the wave set-up is of the order of 10 cm for offshore waves of 4 m. On the contrary, no major correlation is found between the water level and the infragravity significant wave height.

The oceanographic dataset provides, for the first time, observations of processes that can lead to marine floodings in the Bay of Saint-Malo. Thus, despite the fact that the period of measurements did not encompass any flood event, the wave setup, found negligible at hight tide, is unlikely to be a dominant process responsible for flooding, which precisely occurs at high tide with high tidal coefficients. On the contrary, short and infragravity waves, that remain high at the feet of the dyke, seem to have a major impact and can be responsible for overtopping, that is often observed but unfortunately not measured.

## 4.2 Implementation of numerical configuration for a local warning coastal flooding system

One of the objectives of the PAPI for the Saint Malo Agglomeration is to evaluate the feasibility and interest of setting up a local marine flood forecasting system with respect to the national system. In addition of improving the knowledge of the processes responsible for the flooding in this area, the data presented in this paper are the essential prelude to the implementation and calibration/validation of the hydrodynamic models that underlay this forecasting service. We present here an overview of this system, which is currently the subject of ongoing efforts.

The tide, surge and wave modeling of the French national system are based on the barotropic circulation model Hycom (Baraille and Filatoff, 1995) and on the wave model Wavewatch III (R) (hereinafter WW3, The WAVEWATCH III (R) Development Group, 2016), coupled with the Oasis coupler (Valcke et al., 2015).

The French Atlantic configuration (hereinafter called HR) that is operationally run in the Meteo-France storm surge forecast system has a resolution of 600m at nearshore scale that is insufficient for forecasting flooding at the scale of a city like Saint-Malo. In the context of the PAPI, nested grids for both wave and surge models were generated with resolutions of up to 30 m at the coastline (the same methodology for Pertuis-Charentes is described in (Michaud et al., 2015; Pasquet et al., 2021)). The Oasis coupler was used to provide boundary conditions between the Hycom nested configurations, as well as the coupling between the 30m resolution onshore WW3 and Hycom configurations. The overall system relies on curvilinear grids for Hycom and unstructured grids for WW3. The bathymetry part of the coastal 20m-resolution TBDTM referenced to mean sea level, presented in this paper, was interpolated on the curvilinear Hycom grids (whose onshore limits are the coastline) and

the WW3 mesh. This unstructured mesh was generated using Polymesh 2-D Mesh Generator, developed at BGS IT&E. The mesh resolution varies throughout the domain from 50m offshore to 30m onshore, due to the mesh criteria chosen in relation to depth gradient and CFL to optimize node distribution. The coupling follows the vortex-force approach (Ardhuin et al., 2008; Bennis et al., 2011; Michaud et al., 2012), and the exchanges of all the variables (the current, water level and mask variables from Hycom and sea-state variables from WW3) are done every 10 minutes. This modeling system, called THR, allows to represent some nearshore processes such as wave breaking and wave set-up, thanks to the high resolution and the coupling between models.

It is worth noting that the high resolution of the TBDTM (5 m) and the spatial density of the dataset would allow a setup of the model with refined computational grids. The choice of the resolution at the coast is a good compromise considering the (phase-averaged) modelling approach adopted here, practical aspects regarding model implementation and the computational cost. First, a finer resolution would have been too costly for operational purposes. Second, increasing the resolution at the coast with nested grids would require an additional intermediate grid in Hycom. Finally a phase-resolving modelling approach, allowing an explicit representation of the free surface, and a better representation of wave transformations on a coastal scale, would be more appropriate at higher resolution. Such models are currently too expensive for operational use at a national level, although benefiting from active developments on the numerics to reduce their computational cost (Couderc et al., 2017; Marsaleix et al., 2019; Duran et al., 2020; Richard, 2021).

Models were calibrated and validated using the series of measurements in Saint-Malo bay (Seyfried et al., 2021). The breaking index was set to 0.5 in the WW3 configuration. The bottom stress parameterization in Hycom uses a semi-quadratic formulation with bottom drag coefficients maps obtained using stochastic optimization based on - and assessed with - water level observations or predictions.

This modelling system allow the observation of the wave field transformation at the entrance to Saint-Malo Bay with an eastern part of the bay highly exposed, and a western part less exposed as it is protected by Cezembre Island (Figure 7.A. for the December 9, 2018 storm at high tide). The significant wave height decreases from the entrance to the bay to the foot of the dykes mainly due to wave breaking in the Saint-Malo bay and interactions with the numerous obstacles (islands, shoals, groynes). The spatial variability of $H_{m0}$ is well represented for this event, as shown by the comparison with observation points. The simulated surge (atmospherical and wave setup) during the December 9 storm at high tide shows a gradient from the open sea to the coast particularly marked close to the shore defences, after the breaking zone (Figure 7.B.), linked to the generation of a wave setup. In the estuary and outer harbor, the effect of the wave setup is negligible. Comparison with the observation points shows an underestimation of the surge offshore, but a good representation of the surge increase at the foot of the structures (moorings T1-1 and T4-1). The model depicts lower surges at certain points in the bay, particularly in some shoals, which are areas of shallow water that induce a shoaling and a set-down. This is also observed at moorings T3-3 and T3-4 which are positioned on shoals, where there are lower surges than at other moorings. However, the resolution of 30 m and uncertainties in data that are of the order of 5 to 10 centimeters, make point-to-point model interpretation and validation difficult.

While being an important process at low tide, simulations and observations reveal that wave setup is negligible at high tide and thus seems to not be a dominant process responsible for coastal flooding (Seyfried et al., 2021). In fact, the observational period did not include any coastal flooding due to major storms, but statistical analysis (Seyfried et al., 2021) and the high tidal range at Saint-Malo mean that coastal flooding occurs during large tides with high tidal coefficients. Certain processes, such as infra-gravitational waves or wave overtopping processes have shown a non-negligible impact on flooding thanks to measurements or observations made during the sea campaign, remain unrepresented in the model. The modelling system developed in this study is thus non sufficient and would need to be complemented at nearshore scale by a phase-resolved model to represent the infra-gravity waves as well as overtopping. However, this modelling system is the necessary link between the models operated at national scale and these high-resolution phase-resolved models.

Additional measurements would therefore be needed to calibrate and validate this phase-resolved model and in particular with cameras, pressure gauges or lidar stations on the dyke, for the wave overtopping measurement. In addition, another strategy based on permanent networks, with low-sampling, low-power systems with continuous data transmission, could also be complemented by model assimilation and machine learning algorithms to adaptively improve forecast accuracy over time and add robustness and resilience to the system. This strategy would include collaborative aspects, involving stakeholders and local authorities, ensuring its success.
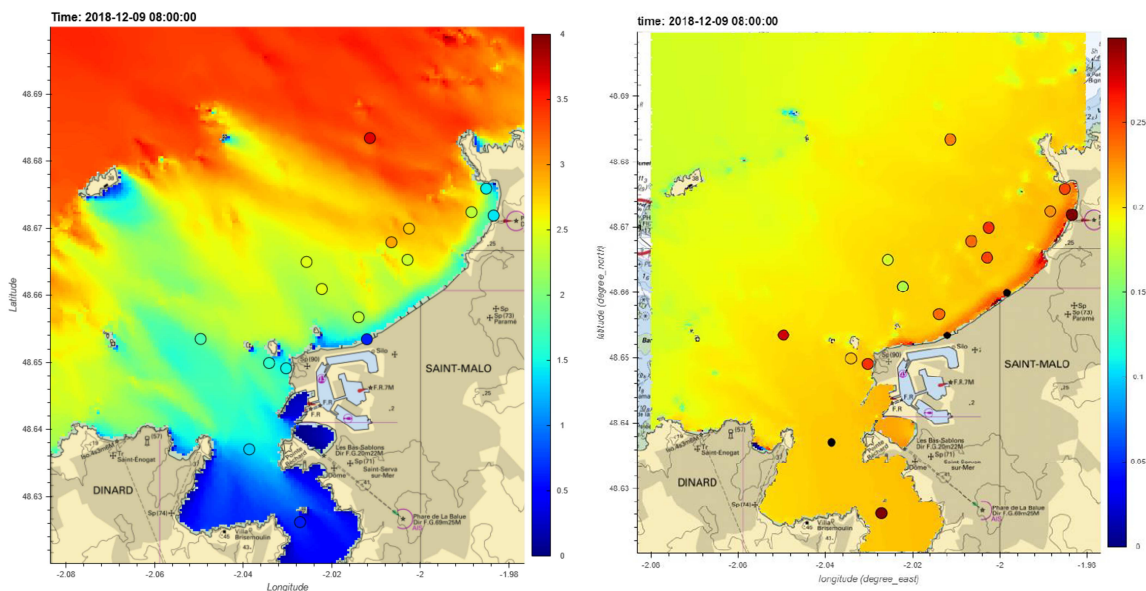
**Figure 7.** Map of significant wave height (up) and surge (atmospherical and wave setup) (bottom) in meters at high tide simulated by the THR system during the December 9, 2018 storm. The color of dots represents the measured value at the various moorings during this event.

## 5  Data availability

The TBDTMs (Shom, 2020a, b) and oceanographic datasets (Shom, 2021) are freely available at doi :

- https://doi.org/10.17183/MNT_COTIER_GNB_PAPI_SM_20m_WGS84

- https://doi.org/10.17183/MNT_COTIER_PORT_SM_PAPI_SM_5m_WGS84

- https://doi.org/10.17183/CAMPAGNE_OCEANO_STMALO

TBDTMs is released through pre-packed files, including:

- files containing bathymetric surfaces, vertically referenced to different vertical datums (Mean Sea Level or Lowest Astronomical Tide) and converted in four grid formats, including NetCDF format (.grd by GMT), Bathymetric Attributed Grid (.bag), ESRI ASCII Raster format (.asc) and ascii text format (.glz)

- a metadata file that contains data sources, geographical extent, legal constraints and a brief summary of the building process, meeting the requirements of the INSPIRE Directive;

- the citation and an associated Digital Object Identifier (unique identifier used to cite scientific articles and datasets) to easily identify the future multiple uses of the DTM;

- the rights and contents report describing the main features of the product and its limitation of use.

Oceanographic dataset is available through four levels of processing, including :

- L0 : direct output of sensors at binary or ascii format.

- L1 : processed outputs of sensors at ascii format using the manufacturers' software.

- L2 : processed data and metadata at NetCDF format.

- L3 : post-processed integrated or peak to peak wave parameters at NetCDF format.

## 6  Conclusions

The acquisition of new topo-bathymetric data in the Bay of Saint-Malo allowed the creation of a topo-bathymetric dataset. This dataset contains two TBDTMs with a resolution of 20 m and 5 m, respectively. An extensive oceanographic campaign was also carried out to create a dataset that provides a set of oceanographic parameters (water levels, currents and sea states) in the Bay of Saint-Malo for different atmospheric, tidal and sea states conditions.

During the oceanographic campaign, three moderate storms occurred in the Bay of Saint-Malo. Their observation allows to analyze the different oceanographic processes involved in coastal flooding specific to this area. The dataset provides, for

the first time, a measurement of the wave transformation in the bay of Saint-Malo, and a quantification of the wave processes at the foot of the protection structures. In this macro-tidal area, the variation of the water level plays a major role on wave processes. At high spring tide, the short and the infragravity waves spread up to the protection structures. The wave set-up is not established, but overtopping by sea pack may occur (not measured).

455

Topo-bathymetric and oceanographic datasets are useful to build, validate and calibrate wave and hydrodynamic models. In the context of the PAPI, a local coastal flood system has been developped to reproduce the surge and waves at high resolution in the Saint-Malo bay. Comparison and calibration with measurements have been made and show that this high-resolution model therefore clearly improves the representation of wave dissipation and surge in the bay, and therefore the national marine

460 flood forecasting system. It provides the right information, refined in resolution and precision, to set up a first level of impact indicators at a local scale. However, some observed processes, such as infra-gravitational waves or wave overtopping remain unrepresented in the model. The coupled system is thus the essential link in the chain to complete the coastal forecasting capability with a phase-resolved model that would enable the modelling of all the processes responsible for a potential flooding event.

465

Finally, although this type of dataset are costly to build and limited in space and time, it enables the characterization of processes at short scales, complementing the satellite altimetry monitoring of coastal variables, which face strong limitations in coastal area. Establishing permanent national networks, with continuous data transmission, complemented by model assimilation and machine learning algorithms to adaptively enhance forecast accuracy over time and add robustness and resilience

470 to the system, seems a promising way forward.

**Appendix A: Surface elevation reconstruction method from bottom pressure**

Three different reconstruction methods were used.

**A1  Hydrostatic reconstruction**

The hydrostatic reconstruction based on the hydrostatic equilibrium (Eq. A1).

475 $\zeta_h = h - h_0 + \delta_m$ (A1)

with $\zeta_h$, the hydrostatic free surface elevation (in m), $h_0$ the mean water depth (in m) and $\delta_m$ the sensor's distance from bed (in m).

## A2 Linear reconstruction

The linear reconstruction based on a transfer function derived from the linear wave theory (TFM) is the most commonly used method (e.g., see Bishop and Donelan, 1987).

$$F\{\zeta_{linear}\} = K_p(\omega)F\{\zeta_h\} \tag{A2}$$

where $F\{\cdot\}$ corresponds to the Fourier transform and $K_p(\omega)$ is the transfer function:

$$K_p(\omega) = \frac{\cosh(k(\omega)h_0)}{\cosh(k(\omega)\delta_m)} \tag{A3}$$

Solving this equation requires the use of the dispersion relation issued from the linear wave theory:

$$\omega^2 = gk\tanh(kh_0) \tag{A4}$$

This method requires an upper cutoff frequency so as to remove high frequency noise that is amplified by the transfer function and to prevent the over-amplification of high frequency energy levels due to non-linear interactions in intermediate and shallow waters (e.g. see Bonneton and Lannes, 2017; Bonneton et al., 2018; Mouragues et al., 2019; Martins et al., 2020). For frequencies exceeding the limit frequency, the correction factor can be replaced by different values: $K_p = 1$ (sharp cut-off, the linear spectrum is replaced by hydrostatic spectrum), linear correction factor, steady correction factor and Jonswap spectrum (see Mouragues et al., 2019, for description of these methods). The optimization of the cut-off frequency and correction factor are a source of improvement in the representation of the wave shape (Mouragues et al., 2019; Martins et al., 2020). In this study, in order to simplify the treatment and make it homogeneous, a sharp cut-off frequency of 0.25 Hz was chosen for the whole dataset.

## A3 Non-linear weakly dispersive reconstruction

The nonlinear weakly dispersive (swnl) reconstruction (Eq. A5) was introduced by Bonneton et al. (2018). This method consists of reconstructing surface wave elevation from non-linear wave theory for weakly dispersive waves.

$$\zeta_{swnl} = \zeta_{swl} - \frac{1}{g}\left[\partial_t(\zeta_{swl}\partial_t\zeta_{swl}) - (\frac{\delta_m}{h_0})^2(\partial_t\zeta_{swl})^2\right] \tag{A5}$$

with $\zeta_{swl}$, the free surface elevation from the linear weakly dispersive reconstruction :

$$\zeta_{swl} = \zeta_h - \frac{h_0}{2g}\left[1 - (\frac{\delta_m}{h_0})^2\right]\partial_t^2\zeta_h \tag{A6}$$

As opposed to the TFM, the resolution of Eq.A5 does not require the use of a dispersion relationship. However, this transform requires intrusion of cutoff frequency to filter the measurement noise (Mouragues et al., 2019). In this study, in order to simplify the treatment and make it homogeneous, a cut-off frequency of $0.5 Hz$ was chosen for the whole dataset. This method allows a better reconstruction of the height of the highest waves near the breaking point (Mouragues et al., 2019), however its

505 application is limited to a weakly dispersive wave regime.

A comparison of free surface elevation with the different methods and with the AST acquisition is shown in figure A1 for high and low tide. $H_{m0}$ is also given for the different methods and sensors.

## Appendix B: Bulk parameters: spectral estimates and wave-by-wave analysis

510 The spectral significant wave height($H_{m0}$), mean periods ($T_{m0n}$) and continuous peak period ($T_{pc}$) were computed using using the $n-th$ moment of the wave spectra ($E$ corresponding to the power spectral density of the elevation signal), which reads:

$$m_n = \int_{f_{min}}^{f_{max}} f^n E(f) df \tag{B1}$$

such that:

$$H_{m0} = 4\sqrt{m_0} \tag{B2}$$

515

$$T_{m0n} = \left(\frac{m_0}{m_n}\right)^{1/n} \tag{B3}$$

$$T_{pc} = \frac{m_{-2}m_1}{m_0^2} \tag{B4}$$

while the discrete peak period was computed from the spectral maximum at the peak frequency $f_{peak}$, as $T_{peak} = 1/f_{peak}$.
520 As an initial approach, the lower bound $f_{min}$ used for computing the moments of the wave spectra was set to 0.04 Hz, note however that a convenient separation between the infragravity band and the gravity band might be defined as half the offshore peak frequency (e.g. see Hamm and Peronnard, 1997; Bertin et al., 2020). The upper bound $f_{max}$ was consistently set to $f_c = 0.2$ Hz for wave pressure gauge and 0.4 Hz for the wave buoys and the AWAC.

525 Considering a well-sampled and detrended timeseries of free surface elevation, an individual wave is defined by convention as the elevation profile between two consecutive instants of downward zero crossing. The height ($H$) of an individual wave is then defined as the difference between the maximum (the crest) and minimum (the trough) values of elevation, while the period ($T$) is the time separating the final instant from the initial instant. In practice a peak is defined as any sample whose two direct neighbours have a smaller amplitude with a minimum distance between two peaks roughly corresponding to a minimum
530 period set to 4 s and a minimum amplitude ($\simeq H/2$) set to 0.1 m. For flat peaks (i.e. more than one sample of equal amplitude wide) the index of the middle sample is returned, rounded down in case the number of samples is even. Given the minimum period and the length of a burst, one can estimate the upper limit of observable waves per burst. If the number of waves actually
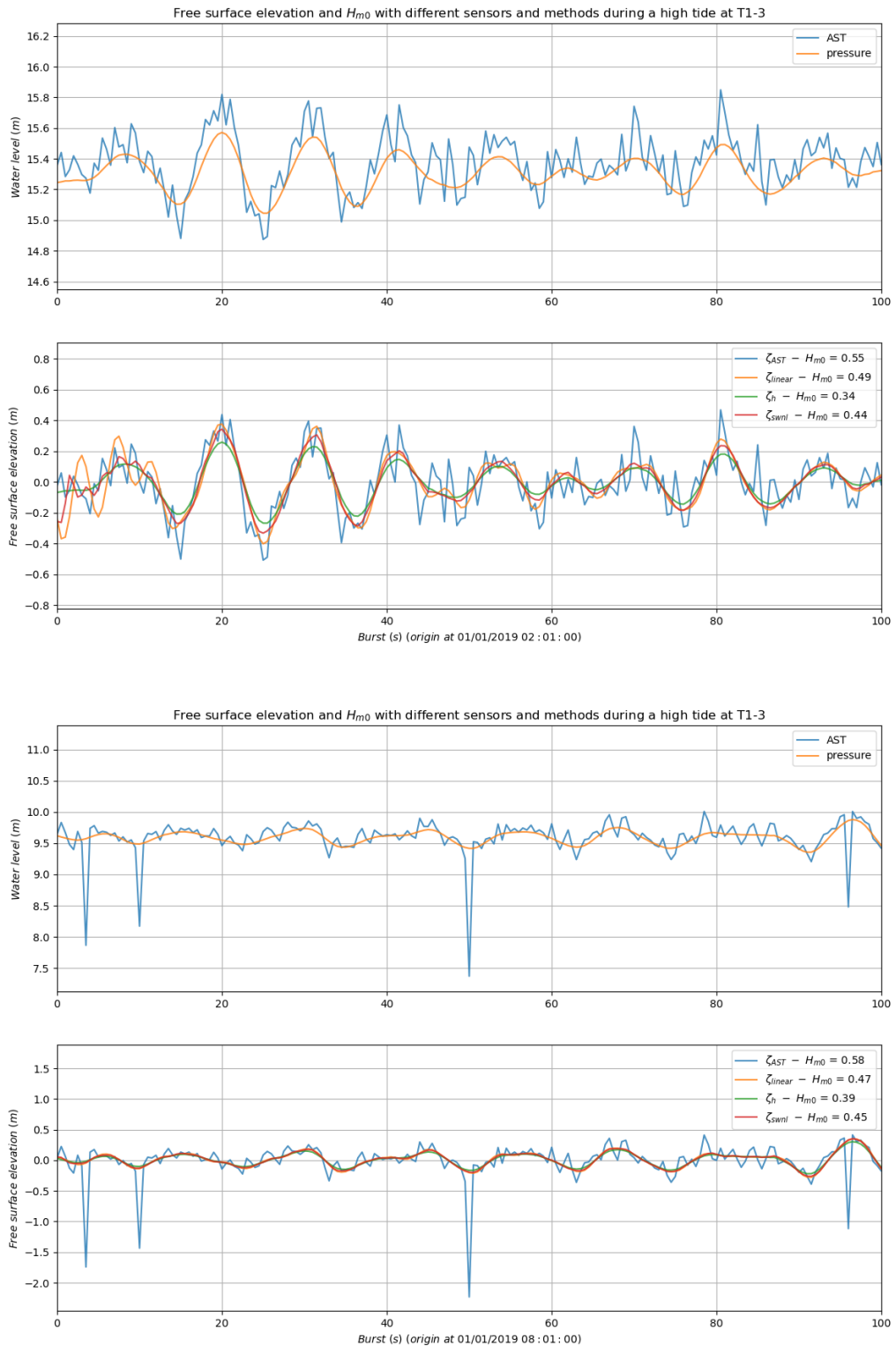
**Figure A1.** Comparison of free surface elevation with the different methods and with the AST acquisition for high (up) and low (bottom) tide. The value of $H_{m0}$ is also given for the different methods

detected does not exceed 10%, the burst is rejected. For $N$ waves detected in the timeseries, the mean wave height ($\overline{H}$) and mean wave period ($\overline{T}$) are given by:

$$\overline{H} = \frac{1}{N} \sum_{i=1}^{N} H_i \tag{B5}$$

$$\overline{T} = \frac{1}{N} \sum_{i=1}^{N} T_i \tag{B6}$$

The significant wave height is computed as the mean value of the top one-third largest waves in the distribution:

$$H_{1/3} = \frac{1}{N/3} \sum_{j=2N/3}^{N} H_j \tag{B7}$$

where $j$ is the index of the waves sorted in ascending order. The maximal wave height ($H_{max}$) is also computed from the wave-by-wave analysis:

$$H_{max} = \max_{i \in [\![1,N]\!]} (H_i) \tag{B8}$$

## Appendix C: Calibration and relocation of the pressure sensors

Calibration is done differently for offshore and foreshore sensors. One solution would be to calibrate them in a laboratory beforehand but pressure sensors are really sensitive to temperature shocks. Transports to the field site can take several weeks or months if it is made by boat, rendering the prior calibration unusable. Another solution is to compare and adjust the data with the atmospheric pressure measurements and this is done easily with sensors on the foreshore, that are pulled out of the water twice a day. For offshore sensors, the only way is to looked at the data before or after being moored.

Another difficulty is in the vertical relocation of the instruments. The vertical positions of the foreshore instruments is obtained with DGPS, whereas the offshore ones are obtained with the sonar ship. To compare the different measurements, one solution is to relocate them in height with respect to the tide gauge of Saint-Malo harbour. Correction factors (slope and offset) from Saint-Malo tide gauge is calculated for each sensor.

*Author contributions.* HM, LB, AP and FL designed the field experiments. LB produced the TBDTMs. LS, HM, MP and AP produced the oceanographic dataset. LS, HM and LB prepared the paper, with contributions from all co-authors.

*Competing interests.* The authors declare that they have no conflict of interest.

*Acknowledgements.* The authors would like to thank the Shom GHOA, IES and Altimétrie littorale teams and all those who participated in the measurement campaign. This research is supported by Shom, Saint-Malo, SMA, Departmental Council of Ille et Vilaine (CD35), Brittany region and the French State. This research is also supported by PROTEVS research program funded by DGA and conducted by Shom. The Litto3D coastal elevation model used for this study is co-produced by IGN and Shom.

# References

Amante, C. J.: Accuracy of interpolated bathymetric digital elevation models, Ph.D. thesis, University of Colorado at Boulder, 2012.

Ardhuin, F., Rascle, N., and Belibassakis, K.: Explicit wave-averaged primitive equations using a generalized Lagrangian mean., Ocean Modelling, 20, 35–60, 2008.

Baraille, R. and Filatoff, N.: Modèle shallow-water multicouches isopycnal de Miami, Tech. Rep. 003/95, Shom, 1995.

Bennis, A., Ardhuin, F., and Dumas, F.: On the coupling of wave and three-dimensional circulation models : Choice of theoretical framework, pratical implementation and adiabatic tests, Ocean Modelling, 40, 260–272, 2011.

Bertin, X., Bruneau, N., Breilh, J.-F., Fortunato, A. B., and Karpytchev, M.: Importance of wave age and resonance in storm surges: The case Xynthia, Bay of Biscay, Ocean Modelling, 42, 16–30, 2012.

Bertin, X., Martins, K., de Bakker, A., Chataigner, T., Guérin, T., Coulombier, T., and de Viron, O.: Energy transfers and reflection of infragravity waves at a dissipative beach under storm waves, Journal of Geophysical Research: Oceans, 125, e2019JC015 714, 2020.

Biscara, L., Maspataud, A., and Schmitt, T.: Generation of bathymetric digital elevation models along French coasts: Coastal risk assessment, Hydro Int, 20, 26–29, 2016.

Bishop, C. T. and Donelan, M. A.: Measuring waves with pressure transducers, Coastal Engineering, 11, 309–328, https://doi.org/10.1016/0378-3839(87)90031-7, 1987.

Bonneton, P. and Lannes, D.: Recovering water wave elevation from pressure measurements, Journal of Fluid Mechanics, 833, 399–429, https://doi.org/10.1017/jfm.2017.666, 2017.

Bonneton, P., Lannes, D., Martins, K., and Michallet, H.: A nonlinear weakly dispersive method for recovering the elevation of irrotational surface waves from pressure measurements, Coastal Engineering, 138, 1–8, https://doi.org/10.1016/j.coastaleng.2018.04.005, 2018.

Bonnot-Courtois, C.: Bay of Mont-Saint-Michel and the Rance Estuary: Recent Development and Evolution of the Depositional Environments, vol. 26, Editions Technip, 2002.

Cariolet, J.: Inondation des côtes basses et risque associés en Bretagne: vers un redéfinition des processus hydrodynamiques liés aux conditions météo-océaniques et des paramètres morpho-sédimentaires, Ph.D. thesis, Brest University, 2011.

Caspar, R., Costa, S., and Jacob, E.: Fronts froids et submersions de tempêtes dans le nord-ouest de la France : le cas des inondations par la mer entre l'estuaire de la Seine et de la Somme, La Météorologie, 57, 37–47, 2007.

Cochet, C. and Lambert, M.: The Rance tidal power plant model, in: In Proceedings of the XXIVth TELEMAC-MASCARET User Conference, 17 to 20 October 2017, Graz University of Technology, Austria, pp. 191–196, 2017.

Conrad, O., Bechtel, B., Bock, M., Dietrich, H., Fischer, E., Gerlitz, L., Wehberg, J., Wichmann, V., and Böhner, J.: System for Automated Geoscientific Analyses (SAGA) v. 2.1.4, Geoscientific Model Development, 8, 1991–2007, https://doi.org/10.5194/gmd-8-1991-2015, 2015.

Couderc, F., Duran, A., and Vila, J.-P.: An explicit asymptotic preserving low Froude scheme for the multilayer shallow water model with density stratification, Journal of Computational Physics, 343, 235—270, 2017.

Crossland, C. J., Kremer, H. H., Lindeboom, H. J., Crossland, J. I. M., and Tissier, M. D. A. L., eds.: Coastal Fluxes in the Anthropocene, Springer Berlin Heidelberg, https://doi.org/10.1007/3-540-27851-6, 2005.

Dagorne, A.: Contribution à l'étude géomorphologique et sédimentologique du littoral de la région de Dinard-Saint-Briac (Ille-et-Vilaine), Ph.D. thesis, Rennes University, 1966.

Dagorne, A.: Le sud du golfe normand-breton: carte sédimentologique des fonds détritiques du prélittoral et répartition du calcaire organogène total., Tech. rep., Doc. Lab. Géomorphologie Dinard, 2., 1968.

Daire, M., Martin, C., and Olmos, P.: Case Study 3H – Côte d'Emeraude, France. Archaeology, Art  Coastal Heritage: Tools to Support Coastal Management (Arch-Manche), Tech. rep., In Satchell, J Tidbury, L (eds) Arch-Manche Technical Report., 2014.

600     Danielson, J. J., Poppenga, S. K., Brock, J. C., Evans, G. A., Tyler, D. J., Gesch, D. B., Thatcher, C. A., and Barras, J. A.: Topobathymetric Elevation Model Development using a New Methodology: Coastal National Elevation Database, Journal of Coastal Research, 76, 75–89, https://doi.org/10.2112/si76-008, 2016.

DHI: Plan de prévention des risques littoraux de Saint Malo, Rapport de phase 2, Tech. rep., DHI, 2016.

Dodet, G., Leckler, F., Sous, D., Ardhuin, F., Filipot, J., and Suanez, S.: Wave Runup Over Steep Rocky Cliffs, Journal of Geophysical
605     Research: Oceans, 123, 7185–7205, https://doi.org/10.1029/2018jc013967, 2018.

Dodet, G., Melet, A., Ardhuin, F., Bertin, X., Idier, D., and Almar, R.: The Contribution of Wind-Generated Waves to Coastal Sea-Level Changes, Surveys in Geophysics, 40, 1563–1601, https://doi.org/10.1007/s10712-019-09557-5, 2019.

Duran, A., Vila, J.-P., and Baraille, R.: Energy-stable staggered schemes for the shallow water equations, Journal of Computational Physics, 401, 2020.

610     Eakins, B. and Taylor, L.: Seamlessly integrating bathymetric and topographic data to support tsunami modeling and forecasting efforts, Ocean globe, pp. 37–56, 2010.

Eakins, B. W. and Grothe, P. R.: Challenges in Building Coastal Digital Elevation Models, Journal of Coastal Research, 297, 942–953, https://doi.org/10.2112/jcoastres-d-13-00192.1, 2014.

Eakins, B. W., Taylor, L. A., Carignan, K. S., and Kenny, M. R.: Advances in Coastal Digital Elevation Models, Eos, Transactions American
615     Geophysical Union, 92, 149–150, https://doi.org/10.1029/2011eo180001, 2011.

Famin, V., Michon, L., and Bourhane, A.: The Comoros archipelago: a right-lateral transform boundary between the Somalia and Lwandle plates, Tectonophysics, 789, 228 539, https://doi.org/10.1016/j.tecto.2020.228539, 2020.

Filipot, J.-F., Roeber, V., Boutet, M., Ody, C., Lathuiliere, C., Louazel, S., Schmitt, T., Ardhuin, F., Lusven, A., Outré, M., et al.: Nearshore wave processes in the Iroise Sea: field measurements and modelling, in: Coastal Dynamics 2013-7th International Conference on Coastal
620     Dynamics, http://www. coastaldynamics2013. fr/pdf_files/055_Filipot_Jean_Francois. pdf, pp. p–605, 2013.

Fox-Kemper, B., Hewitt, H., Xiao, C., Aðalgeirsdóttir, G., Drijfhout, S., Edwards, T., Golledge, N., Hemer, M., Kopp, R., Krinner, G., Mix, A., Notz, D., Nowicki, S., Nurhati, I., Ruiz, L., Sallée, J.-B., Slangen, A., and Yu, Y.: 2021: Ocean, Cryosphere and Sea Level Change. In Climate Change 2021: The Physical Science Basis. Contribution of Working Group I to the Sixth Assessment Report of the Intergovernmental Panel on Climate Change, Cambridge University Press, Cambridge, United Kingdom and New York, NY, USA,
625     https://doi.org/10.1017/9781009157896.011, 2021.

Furgerot, L., Poprawski, Y., Violet, M., Poizot, E., du Bois, P. B., Morillon, M., and Mear, Y.: High-resolution bathymetry of the Alderney Race and its geological and sedimentological description (Raz Blanchard, northwest France), Journal of Maps, 15, 708–718, https://doi.org/10.1080/17445647.2019.1657510, 2019.

Gesch, D. and Wilson, R.: Development of a Seamless Multisource Topographic/Bathymetric Elevation Model of Tampa Bay, Marine Tech-
630     nology Society Journal, 35, 58–64, https://doi.org/10.4031/002533201788058062, 2001.

Hamm, L. and Peronnard, C.: Wave parameters in the nearshore: A clarification, Coastal Engineering, 32, 119 – 135, 1997.

Hébert, H., Abadie, S., Benoit, M., Créach, R., Frère, A., Gailler, A., Garzaglia, S., Hayashi, Y., Loevenbruck, A., Macary, O., et al.: Project TANDEM (Tsunamis in the Atlantic and the English ChaNnel: Definition of the Effects through numerical Modeling)(2014-2018): a

French initiative to draw lessons from the Tohoku-oki tsunami on French coastal nuclear facilities, in: EGU General Assembly Conference Abstracts, p. 6421, 2014.

IHO: IHO Standards for Hydrographic Surveys (Edition 5, 2008), Tech. rep., IHO, https://iho.int/uploads/user/pubs/standards/s-44/S-44_5E.pdf, 2017a.

IHO: Standards of Competence for Category "B" Hydrographic Surveyors (Edition 1.0.1, June 2017), Tech. rep., IHO, https://iho.int/uploads/user/pubs/standards/s-5/S-5B_Ed1.0.1.pdf, 2017b.

IHO: Standards of Competence for Category "A" Hydrographic Surveyors (Edition 1.0.2, June 2018), Tech. rep., IHO, https://iho.int/uploads/user/pubs/standards/s-5/S-5A_Ed1.0.2.pdf, 2018.

Jourdan, D., Paradis, D., Pasquet, A., Michaud, H., Baraille, R., Biscara, L., Dalphinet, A., and Ohl, P.: La phase-3 du projet HOMONIM : définition et contenu, in: XVIèmes Journées, Le Havre, Editions Paralia, https://doi.org/10.5150/jngcgc.2020.087, 2020.

Krogstad, H. E., Gordon, R. L., and Miller, M. C.: High-resolution directional wave spectra from horizontally mounted acoustic Doppler current meters, Journal of Atmospheric and Oceanic Technology, 5, 340–352, 1988.

Le Deunf, J., Schmitt, T., Keramoal, Y., Jarno, R., and Fally, M.: Automating the Management of 300 Years of Ocean Mapping Effort in Order to Improve the Production of Nautical Cartography and Bathymetric Products: Shom's Téthys Workflow., Geomatics, 3, 239–249, https://doi.org/10.3390/jmse8110847, 2023.

Le Menn, M. and Morvan, S.: Velocity Calibration of Doppler Current Profiler Transducers, Journal of Marine Science and Engineering, 8, 847, https://doi.org/10.3390/jmse8110847, 2020.

Louvart, L. and Grateau, C.: The Litto3D project, in: Europe Oceans 2005, IEEE, https://doi.org/10.1109/oceanse.2005.1513237, 2005.

Macnab, R. and Jakobsson, M.: Something old, something new: compiling historic and contemporary data to construct regional bathymetric maps, with the Arctic Ocean as a case study, The International Hydrographic Review, 2000.

Marsaleix, P., Michaud, H., and Estournel, C.: 3D phase-resolved wave modelling with a non-hydrostatic ocean circulation model, Ocean Modelling, 136, 28–50, https://doi.org/https://doi.org/10.1016/j.ocemod.2019.02.002, 2019.

Martins, K., Bonneton, P., Mouragues, A., and Castelle, B.: Non-hydrostatic, Non-linear Processes in the Surf Zone, Journal of Geophysical Research: Oceans, 125, https://doi.org/10.1029/2019jc015521, 2020.

Maspataud, A., Biscara, L., Hébert, H., Schmitt, T., and Créach, R.: Coastal Digital Elevation Models (DEMs) for tsunami hazard assessment on the French coasts, in: EGU General Assembly Conference Abstracts, p. 1590, 2015.

Melet, A., Teatini, P., Cozannet, G. L., Jamet, C., Conversi, A., Benveniste, J., and Almar, R.: Earth Observations for Monitoring Marine Coastal Hazards and Their Drivers, Surveys in Geophysics, 41, 1489–1534, https://doi.org/10.1007/s10712-020-09594-5, 2020.

Michaud, H., Marsaleix, P., Leredde, Y., Estournel, C., Bourrin, F., Lyard, F., Mayet, C., and Ardhuin, F.: Three-dimensional modelling of wave-induced current from the surf zone to the inner shelf, Ocean Science, 8, 657–681, https://doi.org/10.5194/os-8-657-2012, 2012.

Michaud, H., Pasquet, A., Baraille, R., Leckler, F., Aouf, A., Dalphinet, A., Huchet, M., Roland, A., Dutour-Sikiric, M., Ardhuin, F., and Filipot, J.: Implementation of the new French operational coastal wave forecasting system and application to a wave-current interaction study, in: 14th International Workshop on Wave Hindcasting and Forecasting & 5th Coastal Hazard Symposium, 2015.

Michaud, H., Le Goff Le Gourrierec, L., Marsaleix, P., Sous, D., Dealbera, S., Bouchette, F., Bertin, X., Seyfried, L., Leballeur, L., Krien, Y., Meulé, S., Lavaud, L., Estournel, C., Maticka, S., Pasquet, A., Biscara, L., Brosse, F., and Pezerat, M.: Wave transformation on a rocky shore : from field work on Ré Island to 3D modeling, in: Coastal Engineering Proceedings, ICCE2022,37th International Conference on Coastal Engineering, 4-9 december 2022, Sydney Australia, https://doi.org/10.9753/icce.v37.waves.29, 2023.

Mouragues, A., Bonneton, P., Lannes, D., Castelle, B., and Marieu, V.: Field data-based evaluation of methods for recovering surface wave elevation from pressure measurements, Coastal Engineering, 150, 147–159, https://doi.org/10.1016/j.coastaleng.2019.04.006, 2019.

Oltman-Shay, J. and Guza, R.: A data-adaptive ocean wave directional-spectrum estimator for pitch and roll type measurements, Journal of physical oceanography, 14, 1800–1810, 1984.

675 Pasquet, A., Michaud, H., Seyfried, L., Baraille, R., Biscara, L., Y., K., and Jourdan, D.: Improving storm surge and wave forecasts from regional to nearshore scales, in: 9th EuroGOOS Conference, 2021.

Pastol, Y.: Use of Airborne LIDAR Bathymetry for Coastal Hydrographic Surveying: The French Experience, Journal of Coastal Research, 62, 6–18, https://doi.org/10.2112/si_62_2, 2011.

Pineau-Guillou, L. and Dorst, L.: Creation of Vertical Reference Surfaces at Sea Using Altimetry and GPS, in: Reference Frames for Appli-
680 cations in Geosciences, International Association of Geodesy Symposia, vol. 138, https://doi.org/10.1007/978-3-642-32998-2_33, 2013.

Richard, G.: An extension of the Boussinesq-type models to weakly compressible flows, European Journal of Mechanics - B/Fluids, pp. 217–240, 2021.

Seyfried, L., Michaud, H., and Pasquet, A.: Réanalyse et modélisation des surcotes et états de mer, Livrable Shom n°4, PAPI Saint-Malo, Axe 2, Action 2.I, Tech. rep., Shom, 2021.

685 Shom: MNT topo-bathymétrique côtier d'une partie du golfe normand-breton (PAPI Saint-Malo), https://doi.org/10.17183/MNT_COTIER_GNB_PAPI_SM_20M_WGS84, 2020a.

Shom: MNT topo-bathymétrique côtier du port de Saint-Malo et de ses abords (PAPI Saint-Malo), https://doi.org/10.17183/MNT_COTIER_PORT_SM_PAPI_SM_5M_WGS84, 2020b.

Shom: Campagne océanographique in situ aux abords de Saint Malo (Shom), https://doi.org/10.17183/CAMPAGNE_OCEANO_STMALO,
690 2021.

Tawil, T. E., Guillou, N., Charpentier, J.-F., and Benbouzid, M.: On Tidal Current Velocity Vector Time Series Prediction: A Comparative Study for a French High Tidal Energy Potential Site, Journal of Marine Science and Engineering, 7, 46, https://doi.org/10.3390/jmse7020046, 2019.

Tew-Kai, E., Quilfen, V., Cachera, M., and Boutet, M.: Dynamic Coastal-Shelf Seascapes to Support Marine Policies Using Operational
695 Coastal Oceanography: The French Example, Journal of Marine Science and Engineering, 8, 585, https://doi.org/10.3390/jmse8080585, 2020.

The WAVEWATCH III (R) Development Group: User manual and system documentation of WAVEWATCH III R version 5.16. Tech. Note 329, NOAA/NWS/NCEP/MMAB, College Park, MD, USA, 326 pp. + Appendices., 2016.

Valcke, S., Craig, T., and Coquart, L.: OASIS3-MCT User Guide, OASIS3-MCT 3.0, Tech. Rep. TR/CMGC/15/38, CERFACS/CNRS SUC
700 URA No1875, Toulouse, France, 2015.

Wessel, P., Smith, W. H. F., Scharroo, R., Luis, J., and Wobbe, F.: Generic Mapping Tools: Improved Version Released, Eos, Transactions American Geophysical Union, 94, 409–410, https://doi.org/https://doi.org/10.1002/2013EO450001, 2013.

Wong, A. M., Campagnoli, J. G., and Cole, M. A.: Assessing 155 Years of Hydrographic Survey Data for High Resolution Bathymetry Grids, in: OCEANS 2007, IEEE, https://doi.org/10.1109/oceans.2007.4449373, 2007.

705 Woodworth, P. L., Melet, A., Marcos, M., Ray, R. D., Wöppelmann, G., Sasaki, Y. N., Cirano, M., Hibbert, A., Huthnance, J. M., Mon-serrat, S., and Merrifield, M. A.: Forcing Factors Affecting Sea Level Changes at the Coast, Surveys in Geophysics, 40, 1351–1397, https://doi.org/10.1007/s10712-019-09531-1, 2019.